Experimental study on flexural behavior of ECC-concrete composite beams reinforced with FRP bars

Wenjie Ge[a*], Ashraf F. Ashour[b], Dafu Cao[a], Weigang Lu[c],
Peiqi Gao[a], Jiamin Yu[a], Xiang Ji[a], Chen Cai[a]

(a. College of Civil Science and Engineering, Yangzhou University, Yangzhou 225127, China;
b. School of Engineering, University of Bradford, Bradford, BD7 1DP, UK; c. School of Hydraulic, Energy and Power Engineering, Yangzhou University, Yangzhou 225127, China)

Abstract: This paper presents test results of fifteen reinforced engineered cementitious composite (ECC)-concrete beams. The main parameters investigated were the amount and type of reinforcement, and ECC thickness. All reinforced ECC-concrete composite beams tested were classified into four groups according to the amount and type of main longitudinal reinforcement used; three groups were reinforced with FRP, steel and hybrid FRP/steel bars, respectively, having similar tensile capacity, whereas the fourth group had a larger amount of only FRP reinforcement. In each group, four height replacement ratios of ECC to concrete were studied. The test results showed that the moment capacity and stiffness of concrete beams are improved and the crack width can be well controlled when a concrete layer in the tension zone is replaced with an ECC layer of the same thickness. However, the improvement level of ECC-concrete composite beams was controlled by the type and amount of reinforcement used. Based on the simplified constitutive relationships of materials and plane section assumption, three failure modes and their discriminate formulas are developed. Furthermore, simplified formulas for moment capacity calculations are proposed, predicting good agreement with experimental results.

Keywords: ECC, concrete, composite beams, flexural behavior, FRP bars

1 Introduction

The use of fiber reinforced polymer (FRP) composite has gained considerable interest and growing acceptance as internal [1-12] and external reinforcement [13-20] in concrete structures. FRP bars have a high strength-to-weight ratio but low elastic modulus and linear deformation until rupture, leading to brittle failure, larger deflections and crack widths compared with steel reinforced concrete structures. Therefore, serviceability limit state is generally controlling the design of FRP reinforced concrete structures [6-12]. Hybrid reinforced concrete structures [21-28], where FRP reinforcement located closer to the external environment and steel bars embedded in concrete with largest possible cover, combine the advantage of ductility and durability of steel or FRP reinforced concrete structures.

Engineered cementitious composite, a class of high performance cementitious composites with pseudo-strain-hardening behavior and excellent crack control [29, 30], overcomes traditional cement-based materials' softening performance under tensile load by transforming the cracking process from a single macroscopic crack at failure to steady-state multiple micro-cracks. Replacement of concrete in the tension zone around steel longitudinal reinforcement with ECC layer has slightly improved the flexural capacity and deformation ability, but significantly reduced the crack width before yielding of steel reinforcement to be just 20% of that in traditional reinforced

concrete beams [31-35]. FRP reinforced ECC beams showed much better flexural performance in terms of load-carrying capacity, shear resistance, ductility, and damage tolerance compared with FRP reinforced concrete beams [36].

Replacement of concrete in the tension zone around FRP longitudinal reinforcement with an ECC layer is expected to enhance the ductility, reduce deflections and crack widths of FRP reinforced concrete beams owing to the ECC's pseudo-strain-hardening characteristics and excellent crack control ability. In the current investigation, flexural experiments of ECC-concrete composite beams reinforced with FRP bars were conducted and compared with steel and hybrid reinforced beams. Test results including cracks, deflections, failure loads and modes are presented and analyzed. Three failure modes of FRP reinforced ECC-concrete beams were theoretically investigated and simplified formulas for moment capacity were developed. Parametric analysis was also conducted to study the influence of reinforcement ratio and ECC height replacement ratio on the flexural behavior (ultimate moment, ultimate curvature and energy dissipation) of ECC-concrete composite beams.

2 Experimental programs

2.1 Test specimens design

In total, fifteen reinforced ECC-concrete composite beams were cast and tested. The main parameters studied were the amount and type of reinforcement, and ECC layer thickness. The beams were classified into four groups, as shown in Table 1, according to the type and amount of reinforcement. Every group had four specimens with different ECC thickness, except for group SA as SA2 was unexpectedly damaged in the process of testing. A schematic diagram of specimens is shown in figure 1, where the specimen size $b \times h \times l$ =150 mm × 200 mm × 1500 mm, pure flexural span l_m = 400 mm, flexural-shear span l_{mv} = 500 mm, free overhang span l_f = 50 mm, cross-section effective height h_0 = 175 mm, the distance of the center of steel bars to the concrete tensile edge a_s = 25mm, the steel stirrup is Φ8@100, the top steel reinforcement is 2Φ10, h_e is the thickness of ECC, r_h is the ECC height replacement ratio, defined by ECC thickness h_e to the effective height of cross-section h_0, $r_h = h_e / h_0$, and F_u is the total tensile capacity of longitudinal reinforcement. The amount of reinforcement used in the three groups (SA, HA and FA) were selected to achive a similar tensile capacity, F_u, whereas the fourth group (FB) had a larger amount of FRP bars. Each group notation consists of three letters, the first letter identifying the type of reinforcement used, F, S and H for FRP, steel and hybrid reinforcement, respectively, the second letter indicating the tensile capacity of the main longitudinal reinforcement (A or B), whereas the third number representing the ECC height replacement ratio used (1, 2, 3 or 4 represents r_h = 0, 0.29, 0.57 or 1.14, respectively).

Table 1 Specimen design parameters

NO.	steel bars	FRP bars	height replacement ratio r_h	F_u (kN)
FA1/FA2/FA3/FA4	—	2Φ8	0.00/0.29/0.57/1.14	125.60
FB1/FB2/FB3/FB4	—	3Φ8	0.00/0.29/0.57/1.14	188.40
SA1/SA3/SA4	2Φ12	—	0.00/0.57/1.14	136.28

HA1/HA2/HA3/HA4	2⌀10	Φ8	0.00/0.29/0.57/1.14	140.52

Note: ⌀, ⌀ and Φ indicate HRB400 steel, HRB500 steel and FRP reinfoecement, respectively.

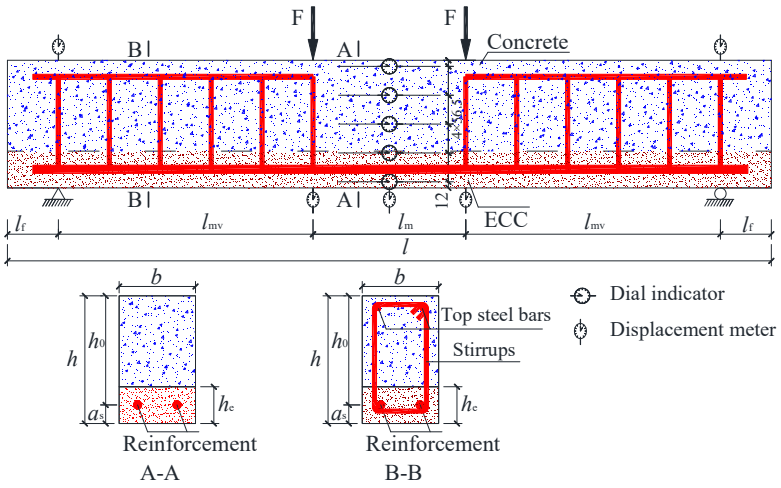

Fig.1 Schematic diagram of reinforced ECC-concrete composite beams

2.2 Test specimens casting and instrumentation

For concrete or ECC beams, concrete or ECC was poured into the mold directly and then vibrated. For ECC-concrete composite beams, layered pouring method was adopted, where ECC was poured into the mold first and vibrated, and then concrete was poured and vibrated.

Displacement gauges were located at mid-span, loading points and supporting points; static resistance strain gauge (TDS-530) was utilized to measure and store the date. The average strain at the mid-span cross-section was measured using five dial indicators located along the height of the cross-section, as shown in figure 1. An oil jack was used to apply the load that was measured by a load sensor. The crack width monitor KON-FK (B) was employed to measure the crack width of the pure flexural span and the crack distribution was depicted on the test specimens by a marker pen.

2.3 Materials

The concrete compressive strength was obtained from testing three 150 mm × 150 mm ×150 mm cube specimens according to the standard for test method of mechanical properties on ordinary concrete GB/T50081-2002 [37] as shown in table 2. The mean values u and coefficients of variation CoV of the cube compressive strength are 47.0 MPa and 0.0112, respectively. Then, the compressive strength f_c, tensile strength f_t and ultimate tensile strain ε_{tu} are 30.16 MPa, 2.55 MPa and 110 × 10^{-6}, respectively as calculated according to the code for design of concrete structures GB50010-2010 [38]. On the other hand, the mechanical properties of steel reinforcement were obtained from testing three specimens according to the standard of metallic materials tensile testing at ambient temperature GB/T228-2002 [39] as presented in table 3. Furthermore, the mechanical properties of ribbed basalt FRP bars were obtained from testing three specimens according to the ACI 440.3R-04 [40]. The stress-strain of FRP bars is shown in figure 2 and its tensile properties are shown in table 3. It is to be noted that the nominal diameter, rib spacing and depth of basalt FRP bars are 8, 16 and 0.8 mm, respectively.

Table 2 Compressive strength of concrete cube

Specimen	Compressive strength		
	f_c (MPa)	u (MPa)	CoV
Specimen 1	47.3		
Specimen 2	47.5	47.0	0.011
Specimen 3	46.3		

Table 3 Mechanical properties of steel and FRP reinforcement

Bars	Diameter (mm)	Yield strength			Ultimate strength			Elastic modulus		
		f_y (MPa)	u (MPa)	CoV	f_u (MPa)	u (MPa)	CoV	E_s (GPa)	u (GPa)	CoV
FRP	8	—	—	—	1273	1250	0.013	50.5	50	0.008
		—			1234			49.5		
		—			1243			50		
HRB400	8	410	406	0.009	489	485	0.006	199	198	0.002
		407			482			198		
		401			485			198		
HRB400	10	402	403	0.003	492	495	0.008	197	198	0.004
		405			493			199		
		403			501			198		
HRB500	12	510	507	0.007	632	630	0.003	200	199	0.002
		508			628			199		
		502			631			199		

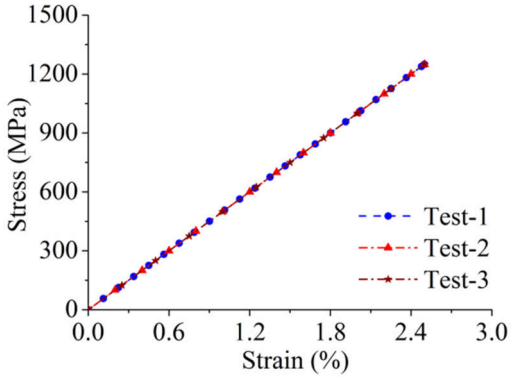

Fig.2 Tensile stress-strain of FRP bar

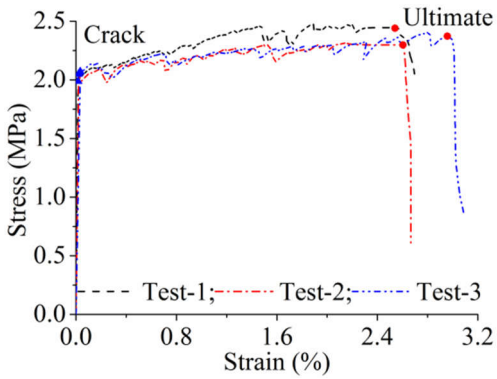

Fig.3 Tensile stress-strain of ECC

Table 4 Tensile properties of ECC

Specimen	ε_{etc}	f_{etc} (MPa)	ε_{etu}	f_{tu} (MPa)
Specimen 1	0.00023	2.0	0.0250	2.4
Specimen 2	0.00025	2.1	0.0260	2.4
Specimen 3	0.00025	2.1	0.0296	2.4

The tensile stress-strain characteristics of ECC presented in figure 3 and table 4 were obtained from testing three rectangular flat-plates of ECC having a size of 160 mm × 40 mm × 15 mm in tension [41], where f_{etc} is the tensile strength at first cracking, f_{tu} is the ultimate tensile strength, ε_{etc} is the tensile strain at first cracking and ε_{etu} is the ultimate tensile strain. On the other hand, the compressive stress-strain curves of ECC shown in figure 4 were obtained from testing three prismatic specimens of ECC

having a size of 40 mm × 40 mm ×160 mm [41], with characteristic values of peak compressive stress f_{ecp} and corresponding strain ε_{ecp} presented in table 5.

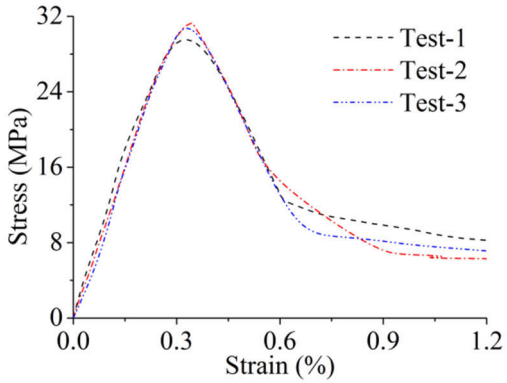

Fig.4 Compressive stress-strain curves

Table 5 Compressive strength of ECC prism

Specimen	Compressive strength			Corresponding strain		
	f_{ecp} (MPa)	u (MPa)	CV	ε_{ecp}(%)	u(%)	CoV
Specimen 1	31.8			0.37		
Specimen 2	30.8	31.4	0.014	0.34	0.36	0.039
Specimen 3	31.6			0.37		

3 Experimental results and discussion

3.1 Average ECC/concrete strain along the height of cross-section

The average ECC/concrete strain distributions along the height of the beam cross-section at various applied moments are shown in figure 5 (for example group FB). The neutral axis height of specimen FB1, FB2 and FB3 moves upward higher than specimen FB4 once the specimen cracked, then moves upward gradually with the applied moment increases.

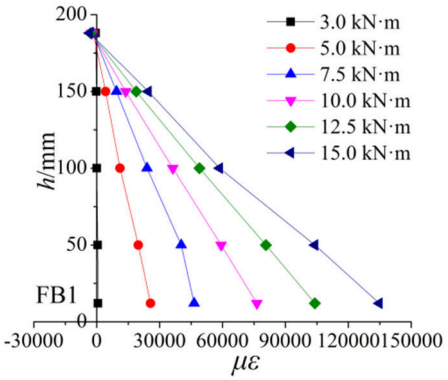

(a) FB1

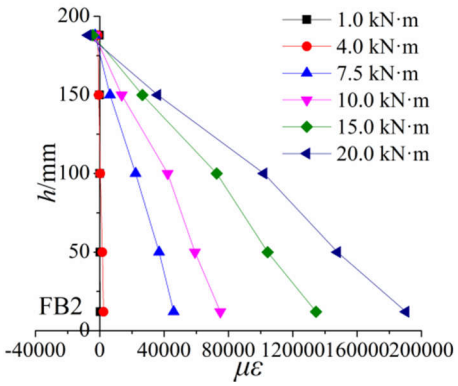

(b) FB2

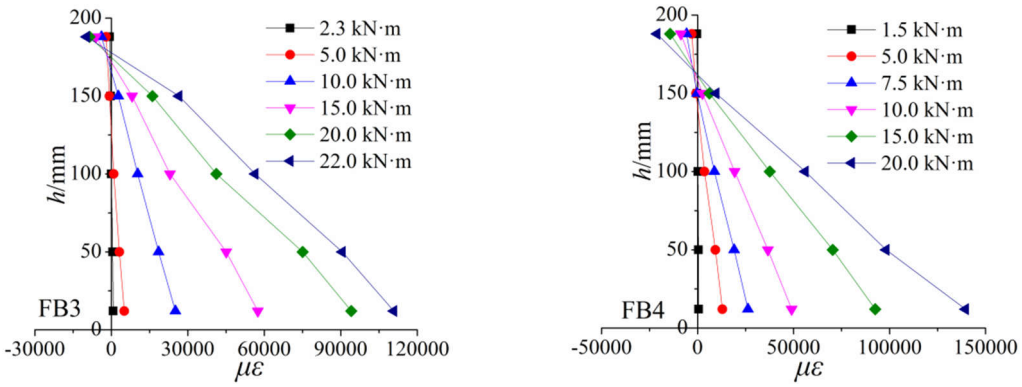

(c) FB3 (d) FB4

Fig.5 Average strain distributions along the height of cross-section

As can be seen from figure 5, the strain distribution is almost linear, indicating:

- the validity of the assumption that plane section perpendicular to the axis of the beam remains plane after loading;
- no delamination between ECC and concrete at various stages of loading.

3.2 Moment-deflection relationship

The mid-span moment-deflection curves of groups FA, FB, SA and HA are shown in figure 6, where f_{lim} is the deflection limit according to the ACI 440.1R-06 [42], θ is the deflection expansion coefficient under long-term loading, and f_{lim} / θ is the deflection limit under short-term loading that is 2.92 mm for FRP reinforced beams tested. The moments and corresponding deflections under short-term loading are shown in table 6, where concrete specimen without ECC layer (FA1, FB1, SA1 and HA1) in each group are taken as control specimen, M_u and f_u are the ultimate moment and corresponding deflection, respectively, M_{qc} is the moment due to the quasi permanent combination of load effects of concrete control specimen in each group and f_{qc} is the corresponding deflection. The ratio of ultimate moment for each specimen to that of the corresponding concrete control specimen M_{ui} / M_{uc} and the ratio of the deflection corresponding to M_{qc} for each specimen to that of the corresponding concrete control specimen f_{qci} / f_{qc} in each group are also presented in table 6.

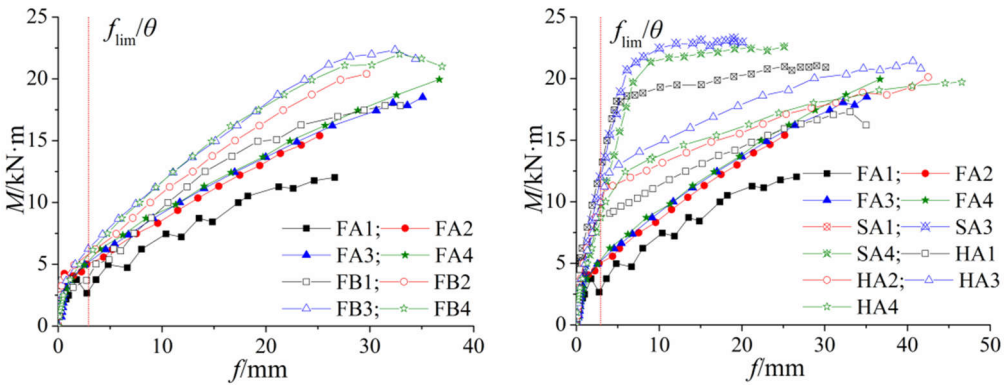

(a) Different reinforcement ratio (b) Different reinforcement form

Fig.6 Mid-span moment-deflection curves under short-term load

Table 6 Comparison of ultimate moment, deflection and crack width

NO.	M_u (kN·m)	M_{ui} / M_{uc}	f_u (mm)	M_{qc} (kN·m)	f_{qc} (mm)	f_{qci} / f_{qc}	ω_{qc} (mm)	ω_{qci} / ω_{qc}
FA1	11.95	1.00	26.11	7.65	12.35	1.00	1.89	1.00
FA2	15.55	1.30	25.53		7.94	0.64	0.84	0.44
FA3	17.57	1.47	30.97		7.23	0.59	0.54	0.29
FA4	18.69	1.56	35.57		6.71	0.54	0.43	0.23
FB1	17.84	1.00	31.48	11.42	12.64	1.00	0.74	1.00
FB2	20.40	1.14	29.69		11.00	0.87	0.51	0.69
FB3	22.34	1.25	32.42		9.64	0.76	0.32	0.43
FB4	22.00	1.23	32.86		9.66	0.76	0.31	0.42
SA1	21.04	1.00	29.00	13.47	4.40	1.00	0.17	1.00
SA3	23.26	1.11	19.00		3.22	0.73	0.08	0.50
SA4	22.60	1.07	25.10		3.47	0.79	0.08	0.48
HA1	17.31	1.00	33.10	11.08	9.32	1.00	0.70	1.00
HA2	20.12	1.16	42.50		3.47	0.37	0.32	0.48
HA3	21.41	1.24	40.66		3.31	0.36	0.31	0.44
HA4	19.71	1.14	46.55		4.59	0.49	0.16	0.22

As can be seen from figure 6 and table 6, the ultimate moments of ECC-concrete beams and ECC beams are higher than that of conventional concrete beams regardless of the reinforcement form. Compared with the control specimen FA1, the ultimate moments of FA2, FA3 and FA4 are improved by 30%, 47% and 56%, respectively. Compared with the control specimen FB1, the ultimate moments of FB2, FB3 and FB4 are improved by 14%, 25% and 23%, respectively. The ultimate moment improvement ratios of group FA are higher than those of group FB, indicating that the ultimate moment improvement ratios decreases with the increase of reinforcement ratio. Compared with the control specimen SA1, the ultimate moments of SA3 and SA4 are improved by 11% and 7%, respectively. Compared with the control specimen HA1, the ultimate moments of HA2, HA3 and HA4 are improved by 16%, 24% and 14%, respectively.

For group FA, the deflections under the quasi permanent load effects combination of FA2, FA3 and FA4 are 64%, 59% and 54% of that of the control specimen FA1, respectively. Similar trends were also observed for groups FB, SA and HA indicating that the stiffness has improved when a layer of ECC is placed in the tension zone. Deflections of FRP reinforced concrete beams (FA1 and FB1), FRP reinforced ECC-concrete composite beams (FA2, FA3, FB2 and FB3) and FRP reinforced ECC beams (FA4 and FB4) cannot meet the requirement of the design code, but, the deflections of specimens FA2, FA3, FA4, FB2, FB3 and FB4 are lower than that of the corresponding control specimen, indicating that, although ECC can improve the ability to resist deformation, specimens still need to be reasonably reinforced with longitudinal reinforcement.

Comparisons of ultimate moments and deflections of specimens of groups SA and HA with respect to the corresponding control specimen of group FA having the same ECC height replacement ratio (groups FA, SA and HA having reinforcement of similar ultimate tensile force) are shown in table 7, where FRP reinforced specimen with the same ECC height replacement ratio (FA1, FA2, FA3 and FA4) are taken as

control specimen, M_q is moment due to the quasi permanent combination of load effects of each specimen and f_q is the corresponding deflection. The ratio of ultimate moment for each specimen to that of the corresponding FRP reinforced control specimen M_{ui} / M_{uf} and the ratio of the deflection corresponding to M_q for each specimen to that of the corresponding FRP reinforced control specimen f_{qi} / f_{qf} are also presented in table 7.

Table 7 Comparison of specimen with similar tensile strength reinforcement

NO.	M_u (kN·m)	M_{ui} / M_{uf}	M_q (kN·m)	f_q (mm)	f_{qi} / f_{qf}	ω_q (mm)	ω_{qi} / ω_{qf}
FA1	11.95	—	7.65	12.35	—	1.89	—
FA2	15.55	—	9.95	12.68	—	1.70	—
FA3	17.57	—	11.24	14.28	—	1.16	—
FA4	18.69	—	11.96	15.58	—	0.61	—
SA1	21.04	1.76	13.47	3.22	0.26	0.17	0.09
SA3	23.26	1.32	14.89	3.87	0.27	0.08	0.07
SA4	22.6	1.21	14.46	4.79	0.31	0.08	0.13
HA1	17.31	1.45	11.08	9.32	0.75	0.70	0.37
HA2	20.12	1.29	12.88	9.54	0.75	0.37	0.21
HA3	21.41	1.22	13.70	6.81	0.48	0.33	0.28
HA4	19.71	1.05	12.61	6.43	0.41	0.16	0.25

As can be seen from table 7, for specimens having reinforcement of similar tensile capacity and the same ECC height replacement ratio, the highest moment capacity was exhibited by steel reinforced beams (group SA), followed by hybrid reinforced beams and then FRP reinforced beams. The moment capacities of specimens SA1, SA3 and SA4 are 76%, 32% and 21%, respectively, higher than that of specimen FA1, FA3 and FA4. The capacities of specimens HA1, HA2, HA3 and HA4 are 45%, 29%, 22% and 5%, respectively, higher than that of specimen FA1, FA2, FA3 and FA4.

However, the deflections of specimens SA1, SA3 and SA4 under quasi permanent load effects combination are 26%, 27% and 31%, respectively, of that of specimens FA1, FA3 and FA4, while the deflections of specimens HA1, HA2, HA3 and HA4 are 75%, 75%, 48% and 41%, respectively, of that of specimens FA1, FA2, FA3 and FA4.

3.3 Maximum crack width under short-term loading

Maximum crack widths at the level of reinforcing bars under short-term loading are shown in figure 7, where $\omega_{max,lim}$ is the crack width limit of concrete structures under long-term loading according to the ACI 440.1R-06 [42]. As the long-term effect of the load combination was not considered in the testing regime, the crack expansion coefficient under long-term load of steel reinforced concrete beams τ_l was taken as reference [38, 43]. So, $\omega_{max,lim}$ / τ_l is the crack width limit under short-term loading, = 0.32 mm for all specimens. The moments and corresponding crack width under short-term loading are shown in table 6, where ω_{qc} is the crack width corresponding to M_{qc}, the ratio of the crack width corresponding to M_{qc} for each specimen to that of the corresponding concrete control specimen ω_{qci} / ω_{qc} in each group is also presented in table 6. The number of cracks n and average crack spacing l_{cr} are also shown in figure

8.

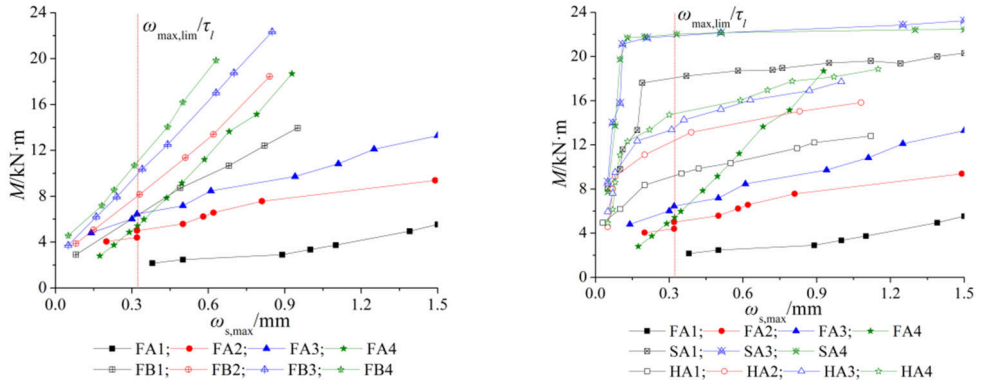

(a) Group FB with respect to FA (b) Groups SA and HA with respect to FA

Fig.7 Maximum crack widths under short-term load

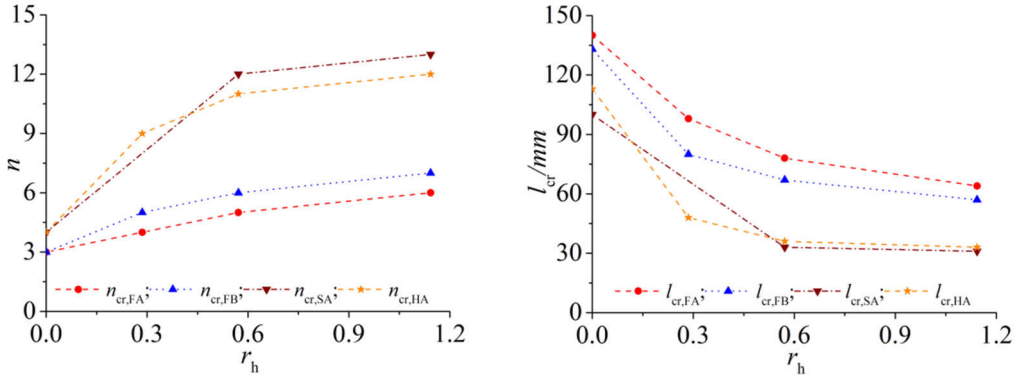

(a) Number of cracks (b) Average crack spacing

Fig.8 Number of cracks and average crack spacing

As can be seen from table 6 and figures 7~8, the number of cracks increases while average crack spacing decreases with the increase of ECC replacement ratio r_h. For FRP reinforced beams, the crack width linearly increases with the load increase. For steel reinforced beams, the crack width linearly increases with the load increase before yielding of steel reinforcement but significantly increases after yielding of steel reinforcement even with no load increase. For hybrid reinforced beams, the crack widths linearly increase with the increase of load before yielding of steel reinforcement. However, the increasing rate becomes faster but lower than that of steel reinforced beams and higher than that of FRP reinforced beams.

The crack widths under quasi permanent load effects combination of FA2, FA3 and FA4 are 44%, 29% and 23%, respectively, of that of concrete control specimen FA1. The crack widths of FB2, FB3 and FB4 are 69%, 43% and 42%, respectively, of that of concrete control specimen FB1. The crack widths of SA2 and SA4 are 50% and 48%, respectively, of that of concrete control specimen SA1. The crack widths of HA2, HA3 and HA4 are 48%, 44% and 22%, respectively, of that of concrete control specimen HA1. The crack widths of ECC-concrete composite beams and ECC beams are lower than that of concrete beams. It is also noted that the crack width decreases with the increase of reinforcement ratio and ECC replacement ratio, and the crack width reduction rate of FRP reinforced beams (group FA) is most remarkable,

indicating that the crack width along the beam can be well controlled when a layer of ECC is placed in the tension zone.

As the reinforcement ratio of the test specimen is low, the crack widths of concrete control specimens FA1, FB1 and HA1 under the quasi permanent combination of load effects cannot meet the serviceability limit state requirements of design code. With the use of ECC, the crack widths of specimens FB3, FB4, HA2, HA3 and HA4 are less $\omega_{max,lim}$ / τ_l required by the ACI 440.1R-06 but specimen FA2, FA3,FA4 and FB2 still cannot meet such requirement. So, although the crack width along the beam can be well controlled when a layer of ECC is placed in the tension zone, specimens still need to be reasonably reinforced to meet the requirement.

For groups having reinforcement of similar tensile capacity, comparisons of crack width under the quasi permanent load effects combination are shown in table 7, where ω_q is the crack width corresponding to M_q. The ratio of the crack width corresponding to M_q for each specimen to that of the corresponding FRP reinforced control specimen ω_{qi} / ω_{qf} is also presented in table 7. As can be seen from table 7, for specimens having reinforcement of similar tensile capacity and the same ECC height replacement ratio, steel reinforced beams (group SA) exhibited the smallest crack width, followed by hybrid reinforced beams (group HA) and, then, FRP reinforced beams (group FA). The crack width of steel reinforced specimens SA1, SA3 and SA4 are 9%, 7% and 13%, respectively, of that of FRP reinforced specimens FA1, FA3 and FA4. On the other hand, the crack width of hybrid reinforced specimens HA1, HA2, HA3 and HA4 are 37%, 21%, 28% and 25%, respectively, of that of FRP reinforced specimens FA1, FA2, FA3 and FA4.

3.4 Failure modes

All specimens exhibited typical flexural failure-characterized by obvious crushing in the compressive zone. For FRP reinforced concrete specimens (for example specimen FA1), large crack width occurred near failure, followed by spalling of concrete in the tensile zone, and, finally, concrete crushed in the compressive zone. For FRP reinforced ECC-concrete composite specimens (for example specimens FA2 and FA3), steel reinforced composite specimens (for example specimen SA3) and hybrid reinforced composite specimens (for example specimen HA3), with further increase of loading, finally, the outermost fiber of concrete in the compression zone reached the ultimate strain and crushed. For FRP reinforced ECC specimens (for example specimen FA4), the outermost fiber of ECC in the compression zone reached the ultimate strain and crushed; however, the fibers in ECC hold the crushed region together. The crack patterns and failure modes of group FA, specimens SA3 and HA3 are shown in figures 9 to 14.

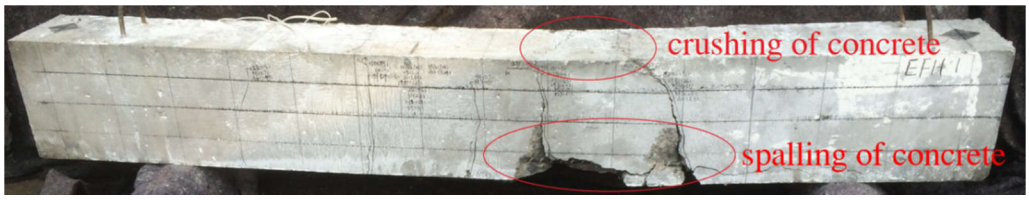

Fig.9 Failure mode of FA1

Fig.10 Failure mode of FA2

Fig.11 Failure mode of FA3

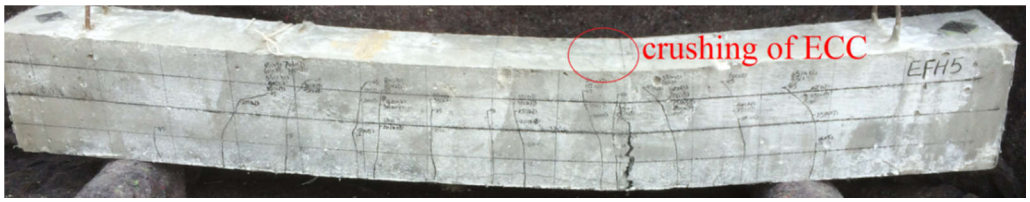

Fig.12 Failure mode of FA4

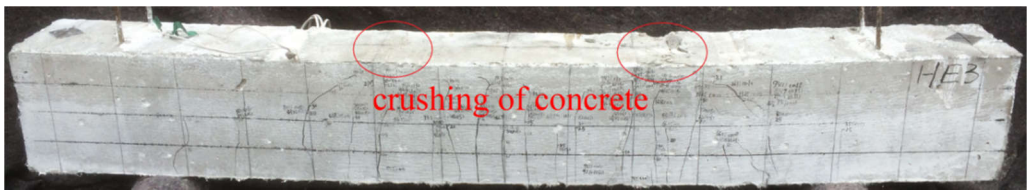

Fig.13 Failure mode of SA3

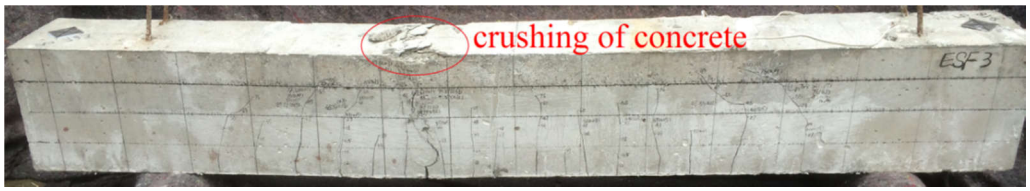

Fig.14 Failure mode of HA3

4 Theoretical analysis

4.1 Failure modes

The moment capacity of FRP reinforced ECC-concrete composite beams can be calculated based on simplified constitutive relationships of materials, compatibility of strains and equilibrium as explained below. According to the constitutive models of materials (concrete, ECC and FRP), failure modes of FRP reinforced ECC-concrete composite beams can be divided into three categories: compressive failure (the compressive strain of concrete reaches its ultimate compressive strain first), tensile failure 1 (the tensile strain of FRP bars reaches its ultimate tensile strain first) and tensile failure 2 (the tensile strain of ECC reaches its ultimate tensile strain first). If the tensile strain in FRP bars / ECC and compressive strain in concrete reach their respective ultimate strain simultaneously, balanced failure occurs. The cross-section strain distribution is shown in figure 15 for various failure modes, where b is the

width of cross-section, h is the height of cross-section, h_s is the distance of FRP bars to the cross-section tensile edge, h_e is the thickness of ECC, h_t is the height of cross-section part in tension (neutral axis depth), h_0 is the effective section height, x_c is the height of cross-section part in compression (concrete above the neutral axis), ε_{et} is the maximum tensile strain in ECC, ε_{ct} is the maximum tensile strain in concrete, ε_c is the maximum compressive strain in concrete and ε_f is the tensile strain in FRP bars.

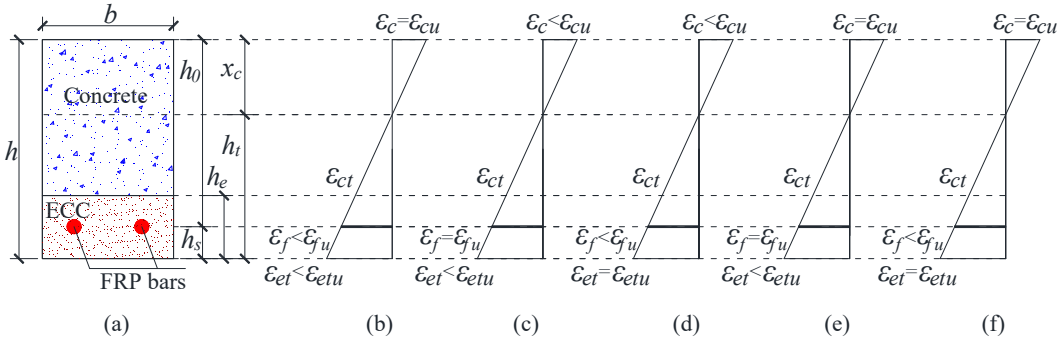

Fig.15 Cross-section strain distribution

In figure 15, the strain distribution corresponding to the three failure modes mentioned above can be identified as below.

1. Compressive failure (figure 15(b)): $\varepsilon_c = \varepsilon_{cu}$, $\varepsilon_f < \varepsilon_{fu}$, $\varepsilon_{et} < \varepsilon_{etu}$.
2. Tensile failure 1 (figure 15(c)): $\varepsilon_c < \varepsilon_{cu}$, $\varepsilon_f = \varepsilon_{fu}$, $\varepsilon_{et} < \varepsilon_{etu}$.
3. Tensile failure 2 (figure 15(d)): $\varepsilon_c < \varepsilon_{cu}$, $\varepsilon_f < \varepsilon_{fu}$, $\varepsilon_{et} = \varepsilon_{etu}$.

When tensile failures 1 and 2 simultaneously occur, $\varepsilon_{fu,b} = \varepsilon_{etu} - (\varepsilon_{etu} + \varepsilon_{cu})\, h_s / h$. So, if $\varepsilon_{fu} = \varepsilon_{fu,b}$, tensile ECC and FRP bars reach their ultimate tensile strain at the same time. If $\varepsilon_{fu} < \varepsilon_{fu,b}$, FRP bars reach its ultimate tensile strain before ECC. If $\varepsilon_{fu} > \varepsilon_{fu,b}$, ECC reaches its ultimate tensile strain before FRP bars.

When compressive failure and tensile failure 1 occur simultaneously, as shown in figure 15(e), balanced failure 1 occurs. Assuming the relative compressive height $\xi_c = x_c / h_0$, the balanced relative compressive height ξ_{cb1} can be calculated according to the plane section assumption.

$$\xi_{cb1} = \frac{x_{c1}}{h_0} = \frac{\varepsilon_{cu}}{\varepsilon_{cu} + \varepsilon_{fu}} \tag{1}$$

When compressive failure and tensile failure 2 occur simultaneously, as shown in figure 15(f), balanced failure 2 occurs and the balanced relative compressive height ξ_{cb2} can be obtained.

$$\xi_{cb2} = \frac{x_c}{h_0} = \frac{x_c}{h} \cdot \frac{h}{h_0} = \frac{\varepsilon_{cu}}{\varepsilon_{cu} + \varepsilon_{etu}} \cdot \frac{h}{h_0} \tag{2}$$

When $\varepsilon_{fu} \le \varepsilon_{fu,b}$, compressive failure occurs for $\xi_c > \xi_{cb1}$ and tensile failure 1 occurs for $\xi_c < \xi_{cb1}$. On the other hand, when $\varepsilon_{fu} > \varepsilon_{fu,b}$, compressive failure occurs for $\xi_c > \xi_{cb2}$ and tensile failure 2 occurs for $\xi_c < \xi_{cb2}$.

According to the force equilibrium of cross-section, the following equation can be obtained.

$$\int_0^{x_c} \sigma_c b dx = \sigma_f A_f + \int_0^{h_e} \sigma_{et} b dx \tag{3}$$

where σ_c is the compressive stress in concrete, σ_f is the tensile stress in FRP bars, A_f is the cross-section area of FRP bars and σ_{et} is the tensile stress in ECC.

For concrete grade less than C50 and considering $\sigma_{et} = f_{etc}$ and $r_h = h_e / h_0$, Eq. (3) can be transformed as below.

For balanced failure 1, $x_c = \varepsilon_{cu} h_0 / (\varepsilon_{cu} + \varepsilon_{fu})$.

$$f_c b h_0 \frac{\varepsilon_{cu} - \varepsilon_{co}/3}{\varepsilon_{cu} + \varepsilon_{fu}} = f_u A_f + f_{etc} b h_e \tag{4}$$

$$\rho_{f,b1} = \frac{f_c}{f_{fu}} \cdot \frac{\varepsilon_{cu} - \varepsilon_{co}/3}{\varepsilon_{cu} + \varepsilon_{fu}} - r_h \frac{f_{etc}}{f_{fu}} \tag{5}$$

$$r_{h,b1} = \frac{f_c}{f_{etc}} \frac{\varepsilon_{cu} - \varepsilon_{co}/3}{\varepsilon_{cu} + \varepsilon_{fu}} - \frac{f_{fu}}{f_{etc}} \rho_f \tag{6}$$

where ε_{co} is the concrete compressive strain corresponding to concrete stress first reaches its compressive strength f_c.

So, if $\rho_f \geq \rho_{f,b1}$ or $r_h \geq r_{h,b1}$, compressive failure occurs. If $\rho_f < \rho_{f,b1}$ or $r_h < r_{h,b1}$, tensile failure 1 occurs.

For balanced failure 2, $x_c = \varepsilon_{cu} h / (\varepsilon_{cu} + \varepsilon_{etu})$, $\varepsilon_f = (\varepsilon_{etu} h_0 - \varepsilon_{cu} h_s) / h$.

$$f_c b h_0 \frac{\varepsilon_{cu} - \varepsilon_{co}/3}{\varepsilon_{cu} + \varepsilon_{etu}} = E_f A_f \frac{\varepsilon_{etu} h_0 - \varepsilon_{cu} h_s}{h} + f_{etc} b h_e \tag{7}$$

$$\rho_{f,b2} = \frac{f_c \frac{\varepsilon_{cu} - \varepsilon_{co}/3}{\varepsilon_{cu} + \varepsilon_{etu}} - f_{etc} r_h}{E_f \frac{\varepsilon_{etu} h_0 - \varepsilon_{cu} h_s}{h}} \tag{8}$$

$$r_{h,b2} = \frac{f_c}{f_{etc}} \frac{\varepsilon_{cu} - \varepsilon_{co}/3}{\varepsilon_{cu} + \varepsilon_{etu}} - \frac{\rho_f E_f}{f_{etc}} \frac{\varepsilon_{etu} h_0 - \varepsilon_{cu} h_s}{h} \tag{9}$$

So, if $\rho_f \geq \rho_{f,b2}$ or $r_h \geq r_{h,b2}$, compressive failure occurs. If $\rho_f < \rho_{f,b2}$ or $r_h < r_{h,b2}$, tensile failure 2 occurs.

4.2 Simplified calculations for ultimate moment

Simplified stress distributions of FRP reinforced ECC-concrete composite beams are shown in figure 16, where α_c is a coefficient relates to the simplified concrete stress distribution.

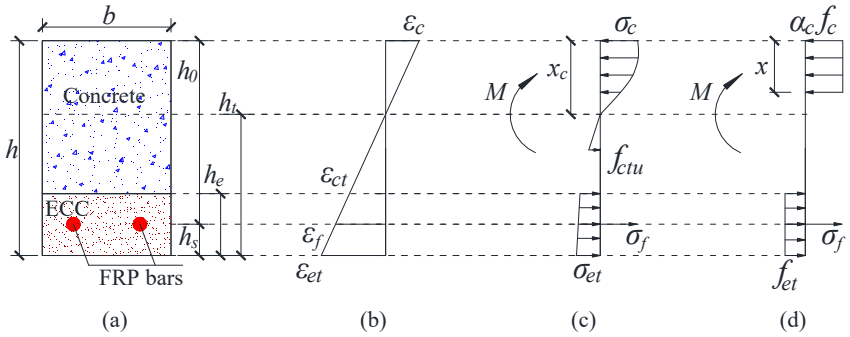

Fig.16 Simplified stress distributions

In case of compressive failure, following equations can be obtained.

$$\alpha_c f_c b x = E_f \varepsilon_f A_f + f_{etc} b h_e \tag{10}$$

$$\varepsilon_f = \varepsilon_{cu}(\beta_c / \xi - 1) \tag{11}$$

Combining equations (10) and (11), the relative compressive height can be calculated as below.

$$\xi_f = \frac{-B_h + \sqrt{B_h^2 - 4A_h C_h}}{2A_h} \tag{12}$$

where, $A_h = \alpha_c f_c$, $B_h = E_f \varepsilon_{cu} \rho_f - f_{etc} r_h$, $C_h = -E_f \rho_f \varepsilon_{cu} \beta_c$.

The flexural capacity of FRP reinforced composite beams, when compressive failure occurs, can be calculated by the following simplified formula.

$$\begin{aligned} M_u &= E_f \varepsilon_f A_f (1 - \xi_f / 2) h_0 + f_{etc} b h_e (h - h_e / 2 - \xi_f h_0 / 2) \\ &= \alpha_c f_c b h_0^2 \xi_f (1 - \xi_f / 2) - f_{etc} b h_e (h_e / 2 - h_s / 2) \end{aligned} \tag{13}$$

When tensile failure 2 occurs, the corresponding tensile strain of FRP bars can be calculated as below.

$$\varepsilon_f = \varepsilon_{etu} \frac{\beta_c - \xi}{\beta_c h / h_0 - \xi} \tag{14}$$

Combining equations (10) and (14), the relative compressive height can be calculated as below.

$$\xi_e = \frac{-B_e + \sqrt{B_e^2 - 4A_e C_e}}{2A_e} \tag{15}$$

where, $A_e = \alpha_c f_c$, $B_e = -(\alpha_c f_c \beta_c h / h_0 + E_f \rho_f \varepsilon_{etu} + f_{etc} r_h)$, $C_e = (E_f \rho_f \varepsilon_{etu} \beta_c + f_{etc} r_h \beta_c h / h_0)$.

The flexural capacity of FRP reinforced composite beams, when ECC tensile failure occurs, can be calculated by the following simplified formula.

$$\begin{aligned} M_u &= E_f \varepsilon_f A_f (1 - \xi_e / 2) h_0 + f_{etc} b h_e (h - h_e / 2 - \xi_e h_0 / 2) \\ &= \alpha_c f_c b h_0^2 \xi_e (1 - \xi_e / 2) - f_{etc} b h_e (h_e / 2 - h_s / 2) \end{aligned} \tag{16}$$

Tensile failure 1 is a brittle failure and should not be allowed in practice; it can be avoided by controlling the FRP reinforcement ratio.

As concrete tensile stress was neglected when calculating the ultimate moment of concrete beams [38], the simplified formula can be also used for FRP reinforced concrete beams ($f_{ect} = 0$).

Comparison of experimental and calculated ultimate moment are presented in table 8, where ρ_f is the FRP reinforcement ratio, r_h is the ECC height replacement ratio, $\rho_{f,b}$ is the balanced FRP reinforcement ratio, $r_{h,b}$ is the balanced ECC height replacement ratio (the calculate values of $r_{h,b}$ of groups FA and FB are negative, for all specimens of groups FA and FB, $r_h \geq r_{h,b}$, indicating that all specimen incur compressive failure), $M_{u,c}$ and $M_{u,e}$ are the calculated and experimental ultimate moment, respectively.

Table 8 Comparison of ultimate moment

NO.	ρ_f(%)	r_h	$\rho_{f,b}$ (%)	$r_{h,b}$	$M_{u,c}$ (kN·m)	$M_{u,e}$ (kN·m)	$M_{u,c}$ / $M_{u,e}$
FA1	0.38	0.00	0.26	—	15.56	11.95	1.30
FA2	0.38	0.29	0.21	—	16.46	15.55	1.06
FA3	0.38	0.57	0.16	—	16.70	17.57	0.95
FB1	0.57	0.00	0.26	—	18.47	17.84	1.04
FB2	0.57	0.29	0.21	—	19.32	20.40	0.95
FB3	0.57	0.57	0.16	—	19.48	22.34	0.87
BREC-T[36]	1.23	0.35	0.44	—	95.64	95.63	1.00

The mean values and coefficients of variation of $M_{u,c}$ / $M_{u,e}$ are 1.02 and 0.124, respectively, indicating good agreement between the simplified formula predication and experimental results.

4.3 Load-deflection

The moment-curvature of FRP reinforced ECC-concrete composite beams can be calculated according to the flexural theory of traditional reinforced concrete beams [44, 45] as presented in figure 17. Based on the plane-section assumption and simplified materials constitutive relationships, the stresses in any cross-section can be obtained and expressed as a function of the maximum compressive strain at the edge of cross section ε_c. So, the internal forces of the cross-section are a function of ε_c.

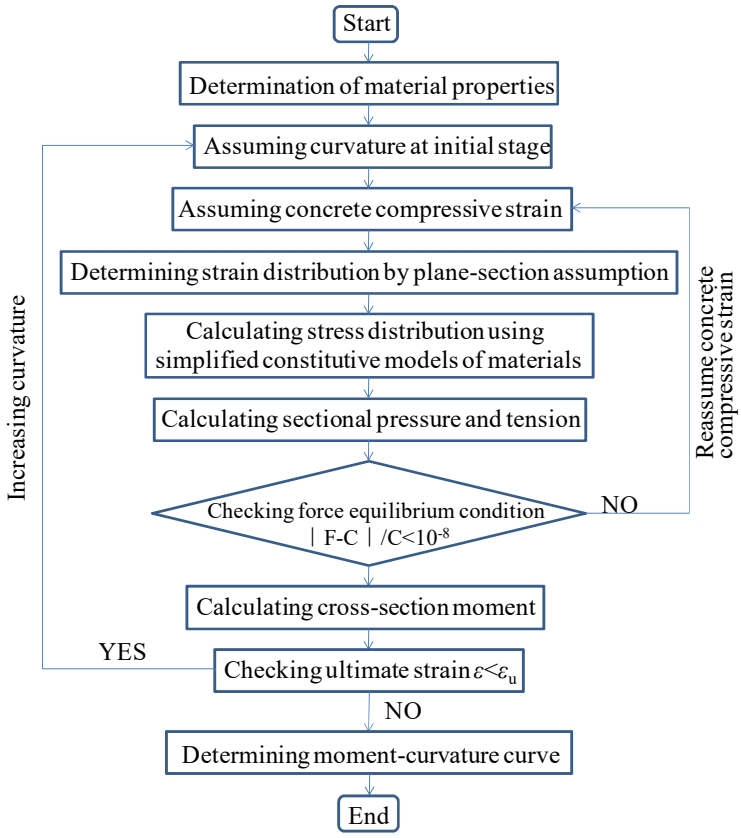

Fig.17 Flow chart for Moment-Curvature calculations

The moment curvature relationship of the composite beam section can be established by the iterative process explained in figure 17. Then, the deflection of mid-span $\delta_{l/2}$ (as shown in figure 18) can be expressed as below [45].

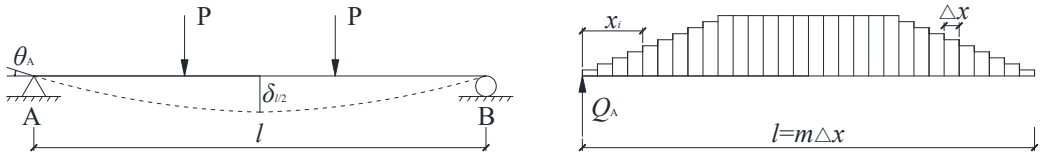

Fig.18 The simply supported beam and corresponding virtual beam

$$\delta_{l/2} = M^{l}_{l/2} = Q_A{}^{l} \frac{l}{2} - \sum_{1}^{m/2} \varphi_i \Delta x (\frac{l}{2} - x_i) \tag{17}$$

where θ_A is the angle of supporting point A, Q_A is the shear force of point A of virtual beam, φ_i is the curvature of each segment, l is the span length of the beam, m is the number of segment (usually more than 16 to ensure acceptable accuracy), Δx is the length of each segment, $\Delta x = l / m$, x_i is the distance of each segment to the supporting point A.

Comparisons of experimental and calculated load-deflection curves for FA1, FA2, FA3 and FA4 are shown in figure 19, indicating good agreements throughout the loading up to the failure.

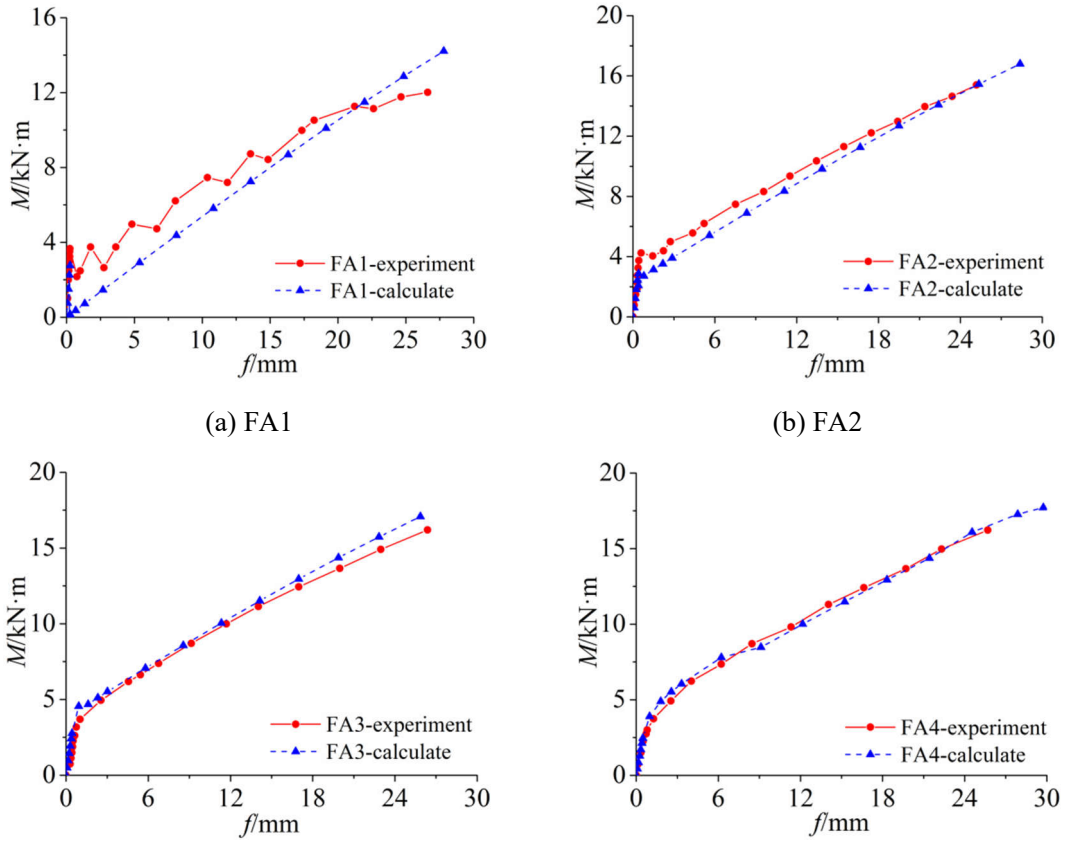

(a) FA1 (b) FA2

(c) FA3 (d) FA4

Fig.19 Comparison of moment-deflection curves

4.4 Parametric analysis

In order to investigate the influence of reinforcement ratio ρ_f and ECC replacement ratio r_h on the flexural behavior of ECC-concrete composite beams, a parametric study is conducted. The basic parameters are as follows: the ECC height replacement ratio r_h is 0.286, the FRP reinforcement ratio ρ_f are 0.11%, 0.22% and 0.32%, f_{fu} = 1250 MPa, E_f = 50 GPa, f_c = 29.6 MPa, f_{etc} = 2.0 MPa, f_{tu} = 2.4 MPa, ε_{etc} = 0.00025, ε_{etu} = 0.025, the cross-section size is the same as that of the test specimens shown in Figure 1. According to section 4.1, the balanced reinforcement ratio $\rho_{f,b}$ of ECC replacement ratio 0.286 is 0.20%. The balanced ECC height replacement ratio $r_{h,b}$ of reinforcement ratio 0.11% and 0.22% are 0.801 and 0.224, respectively.

The influence of ρ_f and r_h on the ultimate moment M_u, ultimate curvature φ_u and energy dissipation E_d (the including area of moment-curvature curves) are shown in figure 20.

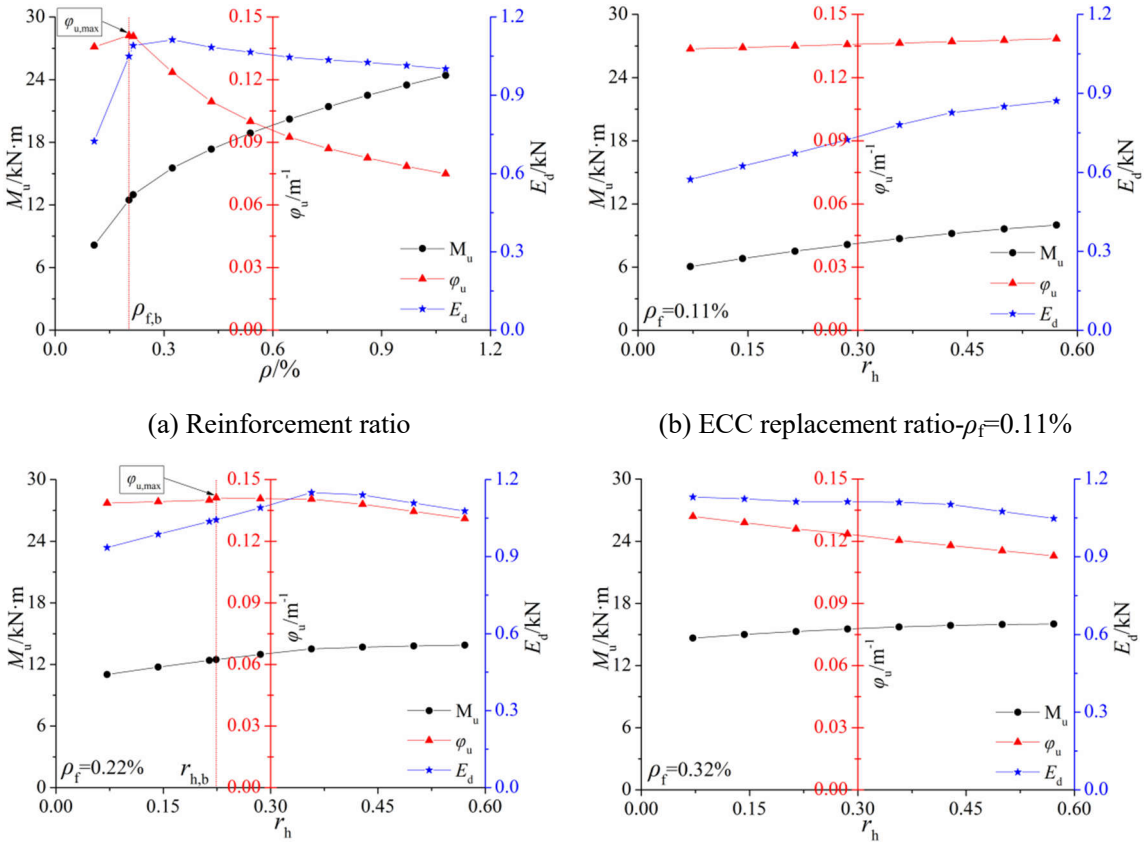

(a) Reinforcement ratio

(b) ECC replacement ratio-ρ_f=0.11%

(c) ECC replacement ratio-ρ_f=0.22%

(d) ECC replacement ratio-ρ_f=0.32%

Fig.20 Parametric analysis

As can be seen from figure 20 (a), with the increasing reinforcement ratio, the ultimate moment significantly increases, the ultimate curvature increases before the balanced reinforcement ratio and then decreases and the energy dissipation, first, increases, and, then, decreases. For composite beams having 0.11% reinforcement ratio, as shown in figure 20 (b), the failure modes are all tensile failure. The ultimate moments, ultimate curvatures and energy dissipations increase with the increase of ECC replacement ratio. For ECC-concrete beams having 0.22% reinforcement ratio, as shown in figure 20 (c), with the increase of ECC replacement ratio, the ultimate moments gradually increase, the ultimate curvatures increase before the balanced ECC height replacement ratio and, then, decrease and the energy dissipations, first, increase and then decrease. For ECC-concrete beams having 0.32% reinforcement ratio, as shown in figure 20 (d), the failure modes are all compressive failure, the ultimate moments gradually increase while the ultimate curvatures and energy dissipations decrease with the increase of ECC replacement ratio.

When the reinforcement ratio (or ECC height replacement ratio) less than balanced reinforcement ratio (or balanced ECC height replacement ratio), tensile failure occurs; in such case, the ultimate moment, ultimate curvature and energy dissipation increase with the increase of tensile resistance (reinforcement ratio or ECC height replacement ratio). On the other hand, when the reinforcement ratio (or ECC height replacement ratio) greater than the balanced reinforcement ratio (or balanced ECC height replacement ratio), compressive failure occurs; the ultimate moment

slightly increases while the ultimate curvature and energy dissipation decrease with the increase of tensile resistance.

5 Conclusions

Based on the experimental study of the flexural behavior of ECC-concrete composite beams reinforced with FRP bars presented above, the following conclusions are drawn:

(1) The ultimate moment capacity and stiffness of reinforced concrete beams are improved and crack width along the beam can be well controlled when a layer of ECC is placed in the tension zone.

(2) For steel reinforced concrete beams, the crack width linearly increases with the load increase before yielding of steel reinforcement but significantly increases after yielding of steel reinforcement even with no load increase. For hybrid reinforced beams, the crack width gradually linearly increases with the increase of load before yielding of steel reinforcement. However, the increase rate becomes faster but still lower than that of steel reinforced beams and higher than that of FRP reinforced beams.

(3) Although the use of ECC layers can improve the ability of reinforced concrete elements to resist cracks and deformation, a minimum amount of longitudinal reinforcement should be used to meet the requirement of serviceability limit state.

(4) Based on the simplified materials constitutive relationships and plane section assumption, three failure modes and their discriminate formulas for ultimate moments are developed. Simplified formulas for ultimate moments are also proposed, giving good predictions compared with experimental results. Moment-deflection predictions are also well compared with these from experiments.

(5) For tensile failure mode, the ultimate moment, ultimate curvature and energy dissipation increase with the increase of tensile resistance. For compressive failure mode, with the increase of tensile resistance, the ultimate moment slightly increases while the ultimate curvature and energy dissipation decrease.

Acknowledgement

The authors appreciate the support of the National Natural Science Foundation of China (51678514, 51308490), the Natural Science Foundation of Jiangsu Province, China (BK20130450), Six Talent Peaks Project of Jiangsu Province (JZ-038, 2016), Graduate Practice Innovation Project of Jiangsu Province (SJCX17-0625), the Jiangsu Government Scholarship for Overseas Studies and Top-level Talents Support Project of Yangzhou University.

References

[1] Masmoudi R, Theriault M, Benmokrane B. Behavior of concrete beams reinforced with deformed fiber-reinforced plastic rods [J]. ACI Structural Journal. 1998, 95(6):665~675.

[2] Peece M, Manfredi G, Cosenza E. Experimental response and code models of GFRP RC beams in bending [J]. Journal of Composites for Construction. 2000, 4(4):182~190.

[3] Gravina RJ, Smith ST. Flexural behavior of indeterminate concrete beams reinforced with FRP bars [J]. Engineering Structures. 2008, 30(9): 2370~2380.
[4] Soric Zorislav, Kisicek Tomislav, Galic Josip. Deflections of concrete beams reinforced with FRP bars [J]. Materials and Structures. 2010, 43(1): 73~90.
[5] Aiello MA, Ombres L. Load-deflection analysis of FRP-reinforced concrete flexural members [J]. Journal of Composites for Construction. 2000, 4(4):164~170.
[6] Houssam Toutanji, YongDeng. Deflection and crack-width prediction of concrete beams reinforced with glass FRP rods [J]. Construction & Building Materials. 2003, 17(1):69-74.
[7] Mohamed S. Issa, Ibrahim M. Metwally, Sherif M. Elzeiny. Influence of fibers on flexural behavior and ductility of concrete beams reinforced with GFRP rebars [J]. Engineering Structures. 2011, 33(5): 1754-1763.
[8] Cristina Barris, Lluis Torres, Jordi Comas, Cristina Mias. Cracking and deflections in GFRP RC beams: An experimental study [J]. Composites Part B: Engineering. 2013, 55(12):580-590.
[9] Maher A. Adam, Mohamed Said, Ahmed A. Mahmoud, Ali S. Shanour. Analytical and experimental flexural behavior of concrete beams reinforced with glass fiber reinforced polymers bars [J]. Construction & Building Materials. 2015, 84(2):354-366.
[10] Andrea Acciai, Angelo D'Ambrisi, Mario De Stefano, Luciano Feo, Francesco Focacci, Raffaele Nudo. Experimental response of FRP reinforced members without transverse reinforcement: Failure modes and design issues [J]. Composites Part B: Engineering. 2016(89): 397-407.
[11] Cristina Barris, Lluis Torres, Irene Vilanova, Cristina Mias, Miquel Llorens. Experimental study on crack width and crack spacing for Glass-FRP reinforced concrete beams [J]. Engineering Structures. 2017(131): 231-242.
[12] Minkwan Ju, Youngwhan Park, Cheolwoo Park. Cracking control comparison in the specifications of serviceability in cracking for FRP reinforced concrete beams [J]. Composite Structures. 2017(182): 674-684.
[13] Philip A. Ritchie, David A. Thomas, Le-Wu Lu, Guy M. Connelly. External Reinforcement of Concrete Beams Using Fibre Reinforced Plastics [J]. Aci Structural Journal. 1991, 88(4):490-500.
[14] Hsuan-Teh Hu, Fu-Ming Lin, Yih-Yuan Jan. Nonlinear finite element analysis of reinforced concrete beams strengthened by fiber-reinforced plastics [J]. Composite Structures. 2004, 63(3):271-281.
[15] Choobbor, S., Hawileh, R. and Abdalla, J. Modeling of Reinforced Concrete Beams Externally Strengthened with a Hybrid Combination of Basalt and Carbon FRP Sheets[C]// The Fourteenth International Conference on Civil, Structural and Environmental Engineering. Sardinia, Italy. 2013.
[16] Hawileh, R., Rasheed, H., Abdalla, J.A., and Tamimi, A. Behavior of reinforced concrete beams strengthened with externally bonded hybrid fiber reinforced polymer systems [J]. Materials & Design. 2014, 53(1): 972-982.
[17] Hee YoungLee, Woo TaiJung, Wonseok Chung. Flexural strengthening of reinforced concrete beams with pre-stressed near surface mounted CFRP systems [J]. Composite Structures. 2017(163): 1-12.
[18] Rongxiong Gao, Qi Cao, Fangjie Hu, Zeyu Gao, FengyangLi. Experimental study on flexural performance of reinforced concrete beams subjected to different plate strengthening [J]. Composite Structures. 2017(176): 565-581.

[19] WensuChen, Thong M.Pham, Henry Sichembe, Li Chen, Hong Hao. Experimental study of flexural behaviour of RC beams strengthened by longitudinal and U-shaped basalt FRP sheet [J]. Composites Part B: Engineering. 2018(134): 114-126.

[20] Xu Yang, Wan-Yang Gao, Jian-Guo Dai, Zhou-Dao Lu, Ke-Quan Yu. Flexural strengthening of RC beams with CFRP grid-reinforced ECC matrix [J]. Composite Structures. 2018(189): 9-26.

[21] Denied Lau, Hoat Joen Pam. Experimental study of hybrid FRP reinforced concrete beams [J]. Engineering Structures. 2010(32): 3857~3865.

[22] Wenjie Ge, Jiwen Zhang, Dafu Cao, Yongming Tu. Flexural behaviors of hybrid concrete beams reinforced with BFRP bars and steel bars[J]. Construction and Building Materials. 2015(87): 28-37.

[23] Hawileh R A. Finite element modeling of reinforced concrete beams with a hybrid combination of steel and aramid reinforcement [J]. Materials & Design. 2015, 65:831-839.

[24] Aiello M A, Ombres L. Structural Performances of Concrete Beams with Hybrid (Fiber-Reinforced Polymer-Steel) Reinforcements [J]. Journal of Composites for Construction. 2002, 6(2):133-140.

[25] Ahmed El Refai, Farid Abed, Abdullah Al-Rahmani. Structural performance and serviceability of concrete beams reinforced with hybrid (GFRP and steel) bars [J]. Construction & Building Materials. 2015(96): 518-529.

[26] Ilker Fatih Kara, Ashraf F. Ashour, Mehmet Alpaslan Körog˘lu. Flexural behavior of hybrid FRP/steel reinforced concrete beams [J]. Composite Structures. 2015(129): 111-121.

[27] Linh V. H. Bui, Boonchai Stitmannaithum, Tamon Ueda. Mechanical performances of concrete beams with hybrid usage of steel and FRP tension reinforcement [J]. Computers & Concrete. 2017, 20(4):391-407.

[28] Renyuan Qin, Ao Zhou, Denvid Lau. Effect of reinforcement ratio on the flexural performance of hybrid FRP reinforced concrete beams [J]. Composites Part B: Engineering. 2017(108): 200-209.

[29] Victor C Li, Shuxin Wang, Cynthia Wu. Tensile strain-hardening behavior of PVA-ECC [J]. ACI Journal of Materials. 2001, 98(6): 483-492.

[30] M Maalej, VC Li. Introduction of strain-hardening engineered cementitious composites in design of reinforced concrete flexural members for improved durability [J]. ACI Structural Journal. 1995, 92(2): 167-176.

[31] M Maalej, S T Quek, S F U Ahmed, J Zhang, V W J Lin, K S Leong. Review of potential structural applications of hybrid fiber Engineered Cementitious Composites [J]. Construction and Building Materials. 2012 (36): 216-227.

[32] Shilang Xu, Nan Wang, Qinghua Li. Experimental study on the flexural performance of concrete beam strengthened with ultra-high toughness cementitious composites [J]. China civil engineering journal, 2010, 43 (5): 17-22.

[33] Xiufang Zhang, Shilang Xu, Hedong Li. Theoretical analysis of flexural performance of plain concrete beams strengthened with ultra-high toughness cementitious composites [J]. China civil engineering journal. 2010, 43 (7): 51-62.

[34] QingHua Li, ShiLang Xu. Experimental investigation and analysis on flexural performance of functionally graded composite beam crack-controlled by ultrahigh toughness cementitious composites [J]. Science in China Series E: Technological Sciences. 2009, 52(6): 1648-1664.

[35] Jun Zhang, Christopher K Y Leung, Yin Nee Cheung. Flexural performance of layered ECC-concrete composite beam [J]. Composites Science and Technology. 2006, 66(11-12): 1501-1512.

[36] Fang Yuan, Jinlong Pan, C. K. Y. Leung. Flexural Behaviors of ECC and Concrete/ECC Composite Beams Reinforced with Basalt Fiber-Reinforced Polymer [J]. Journal of Composites for Construction. 2013.17(5):591-602.

[37] China Academy of Building Research. GB/T50081-2002, Standard for test method of mechanical properties on ordinary concrete[S]. Beijing: China building industry press, 2003.

[38] China Academy of Building Research. Code for design of concrete structures [1] GB50010-2010 [S]. Beijing: China Building Industry Press. 2010.

[39] General Administration of Quality Supervision, Inspection and Quarantine of the People's Republic of China. GB/T228-2002, Metallic materials Tensile testing at ambient temperature[S]. Beijing: Standards press of china. 2002.

[40] American Concrete Institute, Guide Test Methods for Fiber-Reinforced Polymers (FRPs) for Reinforcing or Strengthening Concrete Structures ACI 440.3R-04 [M]. Farmington Hills. Mich, USA, 2004.

[41] Wang Biyuan, Ge Wenjie, Zhou Jingjing, Cao Dafu. Preparation and mechanic behaviors of engineered cementitious composites [J]. Journal of Yangzhou University: Natural science Edition. 2015, 18(3): 64~69.

[42] American Concrete Institute. Guide for the design and construction of structural concrete reinforced with FRP bars ACI 440.1R-06. Detroit: American Concrete Institute. 2006

[43] Yang Yu, Xue Weichen, Zheng Qiaowen. Calculation of crack widths of FRP-reinforced concrete beams [J]. Journal of hydroelectric engineering. 2008, 27(6):79-83.

[44] Doo-Yeol Yoo, Nemkumar Banthia, Young-Soo Yoon. Flexural behavior of ultra-high-performance fiber-reinforced concrete beams reinforced with GFRP and steel rebars [J]. Engineering Structures. 2016 (111): 246-262.

[45] Ge Wenjie. Experimental study and theoretical analysis on concrete beams reinforced with FRP bars blend with steel bars or FRP and steel composite bars [D]. Nanjing: Southeast University, 2009.